Reactions of Group 8, 9, and 10 Monocations (Fe^+, Co^+, Ni^+, Ru^+, Rh^+, Pd^+, Os^+, Ir^+, Pt^+) with Phosphane in the Gas Phase

Ulf Mazurek and Helmut Schwarz*[a]

Dedicated to Professor Gottfried Huttner on the occasion of his 65th birthday

Abstract: The reactions of Group 8, 9 and 10 monocations with phosphane were studied under single-collision conditions in a Fourier transform ion cyclotron resonance (FT-ICR) mass spectrometer. Fe^+ is completely unreactive, Co^+ reacts slowly and shows both adduct formation and P–H bond activation, and Ni^+ reacts slowly as well but shows adduct formation only. In contrast to their first-row congeners, the investigated second- and third-row transition metal monocations show facile P–H bond activations. Remarkably, extensive dehydrogenations of the collision complexes yield cations MPH^+, MP_2^+, MP_3H^+, MP_4^+ and so on. Exceptional behaviour is shown by the two d^9 cations palladium (whose "dehydrogenation power" is rather limited) and platinum (which gives rise to a great manifold of only partially dehydrogenated species as well). Collision-induced dissociation experiments suggest that P_2 and PH units are formed as ligands.

Keywords: bond activation · dehydrogenation · gas-phase reactions · phosphane · transition metals

Introduction

Over the last years, the reactions of phosphane (PH_3) in the gas phase have met increased attention. Reaction partners were H atoms[1] and various cations, for example, Si^+,[2] P^+,[3] PH^+,[4] Cr^+,[5] Fe^+,[6] FeO^+[6] and Pt^+.[7] Further, the formation of transition metal/phosphorus clusters from mixtures of red phosphorus and metal powders has been investigated.[8] $PH_{1-3}^{+/0}$ species themselves have been investigated by ab initio quantum-mechanical calculations.[9] Transition metal monocations show a remarkably diverse reactivity towards phosphane. Cr^+ yields small amounts of the condensation product $CrPH_3^+$, but is unreactive in the sense of P–H bond activation.[5] Fe^+ is unreactive even in the sense of adduct formation, while FeO^+ yields Fe^+, $FeOPH^+$ and $FeOH^+$ in a 2:2:1 ratio.[6] Pt^+ is capable of multiple consecutive P–H bond activation yielding $PtPH^+$, PtP_2^+, PtP_3H^+, PtP_4^+, PtP_5H^+, and PtP_6^+.[7] Due to this diversity, we became interested in a more systematic study of the reactivity of transition metal monocations towards phosphane, and, in this publication, we present the results for Group 8, 9 and 10 elements. To the best of our knowledge, a comprehensive investigation of the gas-phase chemistry of phosphane with Co^+, Ni^+, Ru^+, Rh^+, Pd^+, Os^+ and Ir^+ has not been conducted before. However, the data for Fe^+[6] and Pt^+[7] obtained previously by our group are included in this publication for the purpose of completeness. Furthermore, the Pt^+/PH_3 system has been reinvestigated in the study reported here.

[a] Prof. Dr. H. Schwarz, Dipl.-Chem. U. Mazurek
Institut für Chemie, Technische Universität Berlin
Strasse des 17. Juni 135, 10623 Berlin (Germany)
Fax: (+49) 30-314-21102
E-mail: helmut.schwarz@www.chem.tu-berlin.de

Results and Discussion

Reactant and product neutral species: In general, detection of neutral species is not possible in an FT-ICR mass spectrometer. Consequently, neutral reactants and reaction products have to be inferred from the character of the investigated system. However, with the PH_3 concentration by far exceeding that of all other species present in the reaction cell, this intrinsic problem is reduced to a great extent. For the neutral reactants, all species except phosphane can safely be disregarded because only PH_3 was constantly leaked-in and, thus, was present in the reaction cell in substantial amounts, while all other neutral species (generated from the reactions) can safely be assumed to be removed constantly from the reaction cell by pumping. In terms of formal kinetics, only the PH_3 concentration was so high relative to that of the ions that all reactions can be described to be of pseudo-zeroth order in PH_3, whereas the concentrations of the neutral species generated in the ion-molecule reactions at most reaches the order of the low ions' concentrations.

The composition of neutral reaction products proposed here was based on the difference between reactant and product ion compositions and formal addition of one molecule of phosphane. Based on thermochemical data,[10] the

Table 1. Neutral species originating from reactions of transition metal monocations with phosphane.

	Minimum-energy species	Other possibilities (relative energy $\Delta_r H^\circ_{298}$)[a]
[H]	H	
[H_2]	H_2	2H (104)
[P]	P	
[P,H]	PH	P+H (72)
[P,H_2]	PH_2	P+H_2 (42), PH+H (75), P+2H (146)
[P,H_3]	PH_3	PH+H_2 (55), PH_2+H (84), PH+2H (159), P+3H (231)
[P,H_4]	PH_2+H_2	PH_3+H (20), P+2H_2 (42), PH+H_2+H (75), PH_2+2H (104) P+H_2+2H (146), PH+3H (180), P+4H (251)
[P_2]	P_2	2P (117)

[a] All energies in kcal mol^{-1}.

minimum-energy neutral species was/were assumed to possess the composition as shown in Table 1. The decision was always unequivocal.

Terminology for rate constants: As reported by Brönstrup et al.,[7] the reactions of platinum monocations with phosphane yield dehydrogenated product ions. However, there was no guarantee that the behaviour of other metal cations would parallel that of platinum. In a desire to make different reaction pathways as convenient to compare as possible, the following convention was adopted: In the reaction described by the rate constant $k_{ij\rightarrow kl}$, the reactant ion consisting of the metal cation, i phosphorus and j hydrogen atoms yields the product ion consisting of the metal cation, k phosphorus and l hydrogen atoms (for neutral species involved, see above). This scheme is unequivocal and clear for both $k_{ij\rightarrow kl}$ and $k_{ij\leftarrow kl}$, and the corresponding equilibrium constant $K_{ij\rightleftharpoons kl}$.

Experimental results: While Fe^+ was found to be completely unreactive towards phosphane,[6] both Co^+ and Ni^+ react with phosphane. The respective reactions are slow, and for both cations, the participation of C_5-C_8 hydrocarbons present in the background of the mass spectrometer cannot be ruled out. In fact, numerous signals originating from species $MC_mH_n^+$ (M = Co, Ni) were detected in the m/z range of 135–215. To diminish the hydrocarbons' influence in the kinetic and mechanistic (double-resonance) studies, the Co^+/PH_3 and Ni^+/PH_3 systems were investigated at comparatively high phosphane pressures. Furthermore, kinetic analysis was based on the appearance of the product ions rather than on the consumption of the bare metal cations. However, the reaction efficiencies reported in Table 2 (see below) should be interpreted as upper limits rather than exact values.

Cobalt: The formation of $CoPH_3^+$, CoP_2^+, $CoP_2H_6^+$ and $CoP_3H_3^+$ were observed at a phosphane pressure of 1×10^{-7} mbar. Double-resonance experiments revealed that $CoP_2H_6^+$ was *not* generated from $CoPH_3^+$; this made us conclude that $CoP_2H_6^+$ was generated via at least one Co^+–hydrocarbon complex by phosphane addition and subsequent hydrocarbon/phosphane ligand exchange. On the other hand, $CoPH^+$ (barely observed in the kinetic measurements) and $CoP_2H_2^+$ (never detected in the kinetic measurements) were found to act as direct precursors of $CoP_3H_3^+$, which, in turn, was detected in the kinetic measurements. CoP_2^+ was found to be generated, in part, from $CoP_2H_2^+$. Analysis of the double-resonance experiments leads to the reaction scheme (1); note that species not observed in kinetic measurements are given in parentheses.

Two more comments shall be made about reaction scheme (1): 1) The reaction of Co^+ and background hydrocarbons does not necessarily proceed as a one-step association. Moreover, we focus the mere occurence of this reaction

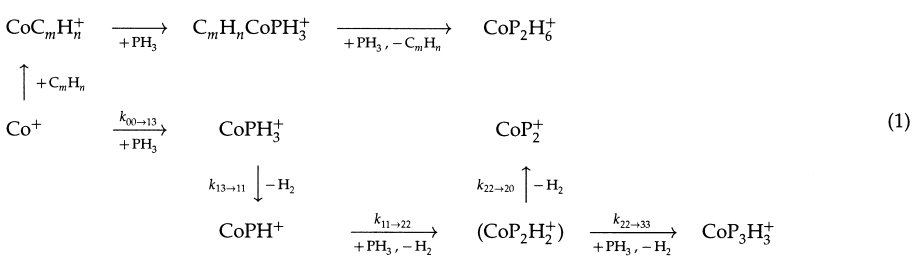

(1)

rather than its acutal mechanism. A related argument applies to the phosphane additions to the $CoC_mH_n^+$ complexes and the phosphane/$C_mH_n^+$ exchange reactions. 2) For principle reasons, the hydrocarbon-mediated generation of $CoPH_3^+$ via the cations $CoC_mH_n^+$ as shown in the reaction sequence (2) cannot be ruled out.

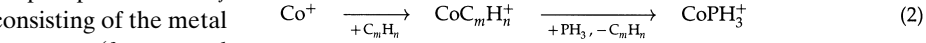

(2)

In contrast, it is likely that the formation of $CoPH_3^+$ proceeds via $CoC_mH_n^+$ because the small (five-atom) system $CoPH_3^+$, when formed directly from Co^+ and PH_3, is unlikely to reach observable concentrations without releasing at least part of the Co^+–PH_3 bond energy by third-body interactions or IR radiation. For the kinetic analysis, however, reactions in sequence (2) were neglected due to their manifold, and the generation of $CoPH_3^+$ was attributed to the formal reaction in scheme (1), while the determination of the rate constant reported here as $k_{00\rightarrow13}$ was solely based on the appearance of $CoPH_3^+$. If, however, the reaction $Co^+\xrightarrow[+PH_3]{k_{00\rightarrow13}}CoPH_3^+$ actually occurs, the reported rate constant would constitute an upper limit rather than an exact value. In order to be consistent, all reactions involving background hydrocarbons were excluded from the kinetic modelling, owing to the unknown partial pressures and the actual contributions of the particular hydrocarbons and their cobalt complexes to the product formation. Rate constants for unimolecular dissociations, namely $k_{13\rightarrow11}$ and $k_{22\rightarrow20}$, could not be determined owing to the incompatible time scales of adduct formation or adduct formation/partial dehydrogenation, respectively, and the loss of molecular hydrogen.

Nickel: The formation of both $NiPH_3^+$ and $NiP_2H_6^+$ was observed at phosphane pressures of both 1×10^{-8} and

  0947-6539/02/0809-2058 $ 20.00+.50/0 *Chem. Eur. J.* **2002**, *8*, No. 9

9×10^{-8} mbar. $NiP_3H_9^+$ was not observed even at the latter phosphane pressure and a reaction time of 128 s. While the adduct formation appears to be straightforward, double-resonance experiments revealed that 1) the species $NiPH^+$, which was never observed in kinetic measurements, seems to be involved to a certain extent in the generation of both $NiPH_3^+$ and $NiP_2H_6^+$ with the actual mechanistic background of the latter reaction pathway remaining unclear, and 2) $NiP_2H_6^+$ is, if at all, only to a small extent being formed from $NiPH_3^+$. The latter observation parallels that for the Co^+/PH_3 system. Consequently, background hydrocarbons were assumed to play a role in the formation of at least $NiP_2H_6^+$, and the rate constant $k_{00\rightarrow13}$ reported here was determined on the basis of the reaction scheme (3) without paying attention to $K_{13\rightleftharpoons11}$, that is, the interconversion of $NiPH_3^+$ and the non-observed $NiPH^+$.

$$\begin{array}{ccccc} NiC_mH_n^+ & \xrightarrow{+PH_3} & C_mH_nNiPH_3^+ & \xrightarrow{+PH_3,\,-C_mH_n} & NiP_2H_6^+ \\ \uparrow{\scriptstyle +C_mH_n} & & & & \uparrow{\scriptstyle ?} \\ Ni^+ & \xrightarrow[+PH_3]{k_{00\rightarrow13}} & NiPH_3^+ & \underset{+PH_3,\,-PH,\;k_{13\leftarrow11}}{\overset{-H_2,\;k_{13\rightarrow11}}{\rightleftharpoons}} & (NiPH^+) \end{array} \quad (3)$$

The determination of rate constants other than $k_{00\rightarrow13}$ seemed inappropriate owing to the unknown contributions of the background hydrocarbons. With respect to these hydrocarbons, the comments made about the Co^+/PH_3 system (see above) apply to nickel as well. The rate constants determined for the reactions of cobalt and nickel monocations with phosphane are summarised in Table 2.

Table 2. Reaction rates and efficiencies for the reactions of atomic Co^+ and Ni^+ with phosphane.[a–c]

Rate constant	Co^+	Ni^+
$k_{00\rightarrow13}$	4.6×10^{-13} (0.035 %)	9.6×10^{-13} (0.074 %)
$k_{11\rightarrow22}$	5.8×10^{-11} (4.8 %)	
$k_{13\rightarrow11}$	n.d.[c]	n.d.
$k_{13\leftarrow11}$		n.d.
$k_{22\rightarrow20}$	n.d.	
$k_{22\rightarrow33}$	5.1×10^{-10} (44 %)	

[a] Fe^+ was found to be completely unreactive towards PH_3.[6] [b] Unless otherwise noted, *reaction rates* are given in units of $cm^3 molecules^{-1} s^{-1}$, whereas *reaction efficiences* ϕ (values given in parentheses) are given as fractions of the experimentally observed rate constant and that according to the capture theory,[19] $\phi = k_{exp}/k_{cap} \times 100\,\%$. [c] n.d. = not determined.

For second- and third-row Group 8, 9 and 10 transition metal monocations, a differentiation between the major reaction sequence, side reactions and adduct formation is indicated. Except for Pd^+ (see below), the *major reaction sequence* is given in scheme (4).

$$\begin{array}{ccccccc} M^+ & \xrightarrow[+PH_3,\,-H_2]{k_{00\rightarrow11}} & MPH^+ & \xrightarrow[+PH_3,\,-2H_2]{k_{11\rightarrow20}} & MP_2^+ & \xrightarrow[+PH_3,\,-H_2]{k_{20\rightarrow31}} & MP_3H^+ \\ & & & & & & \xrightarrow[+PH_3,\,-2H_2]{k_{31\rightarrow40}} \\ MP_4^+ & \xrightarrow[+PH_3,\,-H_2]{k_{40\rightarrow51}} & MP_5H^+ & \xrightarrow[+PH_3,\,-2H_2]{k_{51\rightarrow60}} & MP_6^+ & \xrightarrow[+PH_3,\,-H_2]{k_{60\rightarrow71}} & MP_7H^+ \\ & & & & & & \xrightarrow[+PH_3,\,-2H_2]{k_{71\rightarrow80}} \\ MP_8^+ & \xrightarrow[+PH_3,\,-H_2]{k_{80\rightarrow91}} & MP_9H^+ & & & & \end{array} \quad (4)$$

Note that this reaction sequence is not necessarily completed, that is, the combined phosphane addition/dehydrogenation may stop at a certain product cation depending on the metal centre. This reaction sequence involves maximum dehydrogenation in each reaction step yielding $MP_mH_n^+$ species ($n = m \bmod 2$, that is, $n = 0$ for even and $n = 1$ for odd numbers of m, respectively; mod denotes the *modulo* function), which henceforth are referred to as "hydrogen-poor species". *Side reactions* give rise to "hydrogen-rich species" $MP_mH_n^+$ ($n > m \bmod 2$). Except for platinum (see below), these hydrogen-rich species did not reach significant concentrations. Consequently, we explain their generation by adduct formation followed by rather slow elimination of molecular hydrogen as shown in expressions (5) and (6). As a

$$MP_{i-1}^+ \xrightarrow[+PH_3]{k_{(i-1)0\rightarrow i3}} MP_iH_3^+ \xrightarrow[-H_2]{k_{i3\rightarrow i1}} MP_iH^+ \quad (5)$$

$$MP_{j-1}H^+ \xrightarrow[+PH_3]{k_{(j-1)1\rightarrow j4}} MP_jH_4^+ \xrightarrow[-H_2]{k_{j4\rightarrow j2}} MP_jH_2^+ \xrightarrow[-H_2]{k_{j2\rightarrow j0}} MP_j^+ \quad (6)$$

consequence, the distinction between "major" and "side" reactions may appear to be somehow artificial. However, this distinction may still be indicated when a hydrogen-rich intermediate is observed in a kinetic measurement. Towards the end of a reaction sequence, H_2 elimination may no longer proceed, thus causing *adduct formation* only. Both rate constants and reaction efficiencies are listed in Table 3.

Ruthenium: From Ru^+ through to RuP_6^+, the reaction sequence is straightforward as in reaction sequence (4); hydrogen-rich species are not observed. Besides supporting the reaction mechanism, double-resonance experiments conducted at a phosphane pressure of 1×10^{-8} mbar suggest that the metal centre is ligated by P_2 and PH units. Ejection of RuP_2^+ from the analyser cell causes the signals of Ru^+ and $RuPH^+$ to increase; also the ejection of RuP_3H^+ from the analyser cell leads to an increase of the signals for Ru^+, $RuPH^+$ and RuP_2^+. Similar observations were noted for the other product ions shown in reaction sequence (4). As discussed below in the Experimental Section, we explain these observations as results of unavoidable collisions of the accelerated ions and PH_3 present in the reaction cell as shown in expressions (7) – (9).

At the stage of RuP_6^+, however, the character of the system changes. First, RuP_6^+ accumulates to account for 90 % of the total ion intensity. Second, numerous hydrogen-rich species [see reaction scheme (10) for details] are observed beyond RuP_6^+. Third, while it was possible to derive the rate constants and reaction efficiencies listed in Table 3 from the intensity evolution of the observed species Ru^+ to RuP_5H^+ easily, this no longer holds true for the generation and consumption of RuP_6^+. By applying the model shown in scheme (4), one may reproduce either generation or consumption of that species but not both. From this observation we conclude that some reorganisation of the ligands takes place at the stage of RuP_6^+. Fourth, and backing the "reorganisation hypothesis", double-resonance experiments of

Table 3. Reaction rates and efficiencies for the reactions of second- and third-row Group 8, 9 and 10 monocations with phosphane.[a,b]

Rate constant	Ru^+[c]	Rh^+	Pd^+[d]	Os^+[e]	Ir^+[f]	Pt^+[g]
$k_{00\rightarrow11}$	3.6×10^{-10} (31%)	3.3×10^{-10} (28%)	8.8×10^{-11} (7.4%)	5.0×10^{-10} (45%)	5.6×10^{-10} (50%)	6.6×10^{-10} (59%)
$k_{11\rightarrow20}$	7.4×10^{-10} (64%)	1.1×10^{-9} (97%)	1.9×10^{-10} (17%)	5.0×10^{-10} (45%)	6.6×10^{-10} (60%)	7.8×10^{-10} (71%)
$k_{11\rightarrow22}$			4.7×10^{-10} (41%)		n.d.[b]	2.3×10^{-11} (2.1%)
$k_{20\rightarrow31}$	3.8×10^{-10} (34%)	7.5×10^{-10} (67%)		6.0×10^{-10} (55%)	7.4×10^{-10} (68%)	4.1×10^{-10} (37%)
$k_{22\rightarrow20}$					n.d.	
$k_{31\rightarrow40}$	7.6×10^{-10} (68%)	5.0×10^{-10} (45%)		7.0×10^{-10} (65%)	6.6×10^{-10} (60%)	6.9×10^{-10} (63%)
$k_{31\rightarrow42}$					n.d.	
$k_{40\rightarrow51}$	5.7×10^{-10} (51%)	6.1×10^{-11} (5.5%)		7.8×10^{-10} (72%)	6.7×10^{-10} (62%)	1.3×10^{-10} (12%)
$k_{40\rightarrow53}$		1.1×10^{-11} (0.97%)				2.4×10^{-11} (2.3%)
$k_{42\rightarrow40}$					n.d.	
$k_{51\rightarrow60}$	4.7×10^{-10} (43%)	3.3×10^{-10} (30%)		2.8×10^{-10} (26%)	3.5×10^{-10} (32%)	4.3×10^{-10} (40%)
$k_{53\rightarrow51}$		$6.9\times10^{-8}\ s^{-1}$				$3.4\times10^{-3}\ s^{-1}$
$k_{60\rightarrow71}$	n.d.	1.9×10^{-12} (0.18%)			3.3×10^{-11}[h] (3.1%)	
$k_{60\rightarrow73}$	4.6×10^{-11} (4.2%)	2.1×10^{-11} (1.9%)		4.7×10^{-11} (4.4%)	n.d.	6.7×10^{-12} (0.63%)
$k_{71\rightarrow84}$	n.d.				n.d.	
$k_{73\rightarrow71}$	n.d.			$0.26\ s^{-1}$	n.d.	
$k_{73\rightarrow86}$	n.d.	2.1×10^{-11} (2.0%)		n.d.	n.d.	

[a] Unless otherwise noted, *reaction rates* are given in units of $cm^3 molecules^{-1} s^{-1}$, whereas *reaction efficiences* ϕ (values given in parentheses) are given as fractions of the experimentally observed rate constant and that according to the capture theory,[19] $\phi = k_{exp}/k_{cap}\times100\%$. [b] n.d. = not determined, see text. [c] For additional reactions observed for the $RuP_mH_n^+$ system, see scheme (10) and text. [d] For additional reactions observed for the Pd^+/PH_3 system, see Table 4. [e] For additional reactions observed for the Os^+/PH_3 system, see Table 5. [f] For additional reactions observed for the Ir^+/PH_3 system, see scheme (16) and text. [g] For additional reactions observed for the Pt^+/PH_3 system, see Table 7. [h] Base on the consumption of IrP_6^+ only, that is, the sum of $k_{60\rightarrow71}$ and $k_{60\rightarrow73}$, while ignoring the rise of IrP_7H^+ and $IrP_7H_3^+$; see text.

$$RuP_2^+ \text{ (accelerated)} \xrightarrow[-P_2]{\text{collision with } PH_3} Ru^+ \xrightarrow[+PH_3,\,-H_2]{k_{00\rightarrow11}} RuPH^+ \quad (7)$$

$$RuP_3H^+ \text{ (accelerated)} \xrightarrow[-PH]{\text{collision with } PH_3} RuP_2^+ \quad (8)$$

$$RuP_3H^+ \text{ (accelerated)} \xrightarrow[-P_2]{\text{collision with } PH_3} RuPH^+ \xrightarrow[+PH_3,\,-2H_2]{k_{11\rightarrow20}} RuP_2^+ \quad (9)$$

$RuP_mH_n^+$ species ($m = 6-9$, $n = 0-9$; phosphane pressure 1×10^{-8} mbar, reaction time 192 s) do not give rise to fragment ions with less than six phosphorus atoms. In contrast, ejection of the just-mentioned cations from the reaction cell caused the RuP_6^+ signal to increase. From these observations, we concluded that the phosphorus atoms ligating the ruthenium centre no longer form P_2 units as found for the less-ligated species, that is, RuP_2^+, RuP_3H^+, ... (see discussion of the double-resonance experiments above). In contrast, it appears that units of P_2, PH and PH_3 are lost from the species $RuP_mH_n^+$ ($m = 7-9$, $n = 0-9$) by unavoidable collision-induced dissociation, while the RuP_6^+ core remains intact. Further, the double-resonance experiments reveal that the species $RuP_mH_n^+$ ($m = 7-9$, $n = 0-9$) are in equilibria with each other as summarised in scheme (10). Species not observed in the kinetic measurements are given in parentheses. Interestingly, dehydrogenation predominates even for species $RuP_{8-9}PH_n^+$, except $RuP_8PH_6^+$.

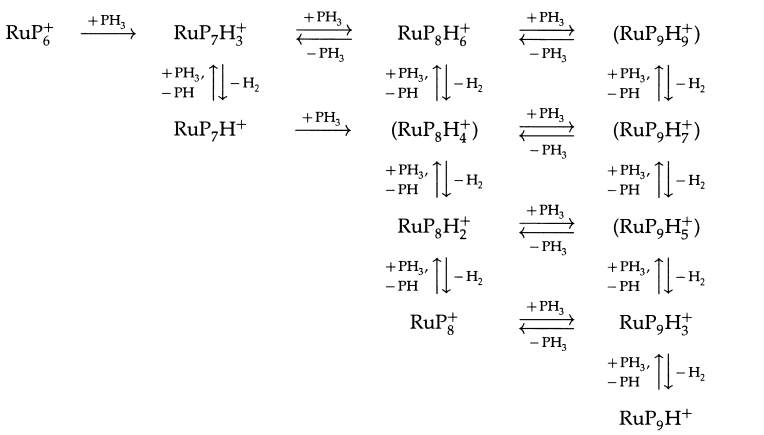

(10)

  0947-6539/02/0809-2060 $ 20.00+.50/0 *Chem. Eur. J.* **2002**, *8*, No. 9

Rhodium: The reaction sequence for rhodium follows that given in scheme (4) from Rh^+ through to RhP_4^+. Species reaching concentrations just surmounting the noise level were $RhPH_3^+$, $RhP_2H_2^+$, $RhP_2H_4^+$, RhP_3^+ and $RhP_3H_3^+$. Similar to RuP_6^+, RhP_4^+ accumulates to about 75% of the total ion intensity and thus dominates the product spectrum at a certain reaction time. Other similarities to the Ru^+/PH_3 system are: 1) The generation and consumption of RhP_4^+ cannot be modelled without assuming at least two isomers with different reactivities towards PH_3 and 2) beyond RhP_4^+, dehydrogenation is no longer complete, and the concentration of $RhP_5H_3^+$ reaches a substantial level. During double-resonance experiments at a reaction time of 32 s and a phosphane pressure of 1×10^{-7} mbar, the only species observed were $RhP_5H_3^+$, RhP_6^+, $RhP_7H_3^+$ and $RhP_8H_6^+$. An additional kinetic study (phosphane pressure 1.5×10^{-8} mbar, max. reaction time 128 s) revealed the generation of RhP_7H^+ in small amounts, while it could not confirm the generation of $RhPH_3^+$, $RhP_2H_2^+$, $RhP_2H_4^+$ and RhP_3^+. Consequently, these four species and the small signal of $RhP_3H_3^+$ were neglected in the kinetic analysis.

Palladium: The reactions observed for palladium cannot be described adequately by scheme (4). In contrast, the reaction sequence (11) applies.

$$\begin{array}{l} \xrightarrow{k_{11\rightarrow20}\ +PH_3,\,-2H_2} PdP_2^+ \xrightarrow{k_{20\rightarrow13}\ +PH_3,\,-P_2} PdPH_3^+ \\ Pd^+ \xrightarrow{k_{00\rightarrow11}\ +PH_3,\,-H_2} PdPH^+ \xrightarrow{k_{11\rightarrow22}\ +PH_3,\,-H_2} PdP_2H_2^+ \xrightarrow{k_{22\rightarrow33}\ +PH_3,\,-H_2} PdP_3H_3^+ \xrightarrow{k_{33\rightarrow26}\ +PH_3,\,-P_2} PdP_2H_6^+ \\ \xrightarrow{k_{11\rightarrow23}\ +PH_3,\,-H} PdP_2H_3^+ \end{array} \quad (11)$$

One might argue that the reaction $PdPH^+ \xrightarrow[+PH_3,\,-H]{k_{11\rightarrow23}} PdP_2H_3^+$ is rather exceptional and unlikely to occur owing to the generation of atomic hydrogen. However, double-resonance experiments showed that $PdP_2H_3^+$ is a follow-up product of $PdPH^+$, whereas no other precursor to $PdP_2H_3^+$ could be detected unequivocally. Consequently, we assume its generation to proceed as shown in sequence (11). On the other hand, the existence of two additional reaction channels shown in scheme (12) could not be proven beyond doubt by double-resonance experiments.

$$PdPH_3^+ \xrightarrow{k_{13\rightarrow22}\ +PH_3,\,-2H_2} PdP_2H_2^+ \xrightarrow{k_{22\rightarrow23}\ +PH_3,\,-PH_2} PdP_2H_3^+ \quad (12)$$

Kinetic analyses including these reaction pathways resulted in rate constants (see Table 4) being at least two orders of magnitude smaller than the ones reported in Table 3. In addition, branching between the three reaction channels shown in sequence (11) remained constant through the formation of the final products. Consequently, these two hypothetical reaction channels were disregarded in the kinetic analysis.

In comparison to the other 4d and 5d metal cations studied here, the "dehydrogenation power" of Pd^+ is rather limited. In addition, the Pd^+–P_2 bond appears to be rather weak, as indicated by the facile replacement of a P_2 unit by a PH_3 ligand as shown for the generation of $PdPH_3^+$ and $PdP_2H_6^+$ in sequence (11).

Table 4. Reaction rates and efficiencies for the Pd^+/PH_3 system.[a–c]

	$k_{11\rightarrow20}$ 1.9×10^{-10} (17%)	$k_{20\rightarrow13}$ 7.4×10^{-10} (66%)	
$k_{00\rightarrow11}$ 8.8×10^{-11} (7.4%)	$k_{11\rightarrow22}$ 4.7×10^{-10} (41%)	$k_{22\rightarrow33}$ 1.4×10^{-10} (12%)	$k_{33\rightarrow26}$ 2.3×10^{-10} (20%)
	$k_{11\rightarrow23}$ 1.1×10^{-10} (9.8%)		
$k_{13\rightarrow22}$ n.d.	$k_{22\rightarrow23}$ n.d.		

[a] The arrangement follows that in scheme (11) whenever possible. [b] Unless otherwise noted, *reaction rates* are given in units of $cm^3 molecules^{-1} s^{-1}$, whereas *reaction efficiences* ϕ (values given in parentheses) are given as fractions of the experimentally observed rate constant and that according to the capture theory,[19] $\phi = k_{exp}/k_{cap} \times 100\%$. [c] n.d. = not determined, see text.

Osmium: The reaction sequence for osmium follows that given in scheme (4) from Os^+ through to OsP_6^+. Similar to RuP_6^+, some reorganisation of the OsP_6^+ ion's ligand sphere appears to occur. While that ion accumulates to more than 70% of the total ion intensity at a certain reaction time, the temporal evolution of its concentration cannot be accounted for by a simple generation–consumption scheme. Beyond OsP_6^+, dehydrogenation is no longer complete. Although both OsP_7H^+ and OsP_8^+ dominate the product ion spectrum, $OsP_7H_3^+$, $OsP_8H_2^+$ and $OsP_8H_6^+$ were observed as well. For ions containing nine phosphorus atoms, $OsP_9H_3^+$ dominates over OsP_9H^+ and $OsP_9H_5^+$. Following the reaction scheme (4) and the adduct formation pathway, we assume the formation of the cations to proceed as shown in sequences (13)–(15).

$$OsP_8^+ \xrightarrow{k_{80\rightarrow91}\ +PH_3,\,-H_2} OsP_9H^+ \quad (13)$$

$$OsP_8^+ \xrightarrow{k_{80\rightarrow93}\ +PH_3} OsP_9H_3^+ \quad (14)$$

$$OsP_8H_2^+ \xrightarrow{k_{82\rightarrow95}\ +PH_3} OsP_9H_5^+ \quad (15)$$

However, the rate constants for these formation reactions were not determined due to the fact that the reaction products were observed, at a phosphane pressure of 1×10^{-8} mbar, only at a reaction time of 128 s. Furthermore, possible interconversions of the species $OsP_9H_n^+$ and the alternative formation of $OsP_9H_3^+$ (e.g., $OsP_8H_2^+ \xrightarrow[+PH_3,\,-H_2]{k_{82\rightarrow93}} OsP_9H_3^+$) were not investigated. Species with more than nine phosphorus atoms were not observed.

For OsP_8^+, we were interested in the ligand structure and arrangement. While single P atoms can be excluded as ligands based on the P–P bond dissociation energy of 117 kcal mol^{-1}

(see Table 1), plausible ligand structures are: 1) P_2 units, 2) one or more phosphorus chains as in red phosphorus and 3) P_4 tetrahedra as in yellow phosphorus. To elucidate the structure of OsP_8^+, it was subjected to a collision-induced dissociation experiment. It turned out that OsP_8^+ looses P_2 units only. No loss of single phosphorus atoms or higher P_n molecules ($n>2$) from the OsP_8^+ ion was observed. We conclude that the Os^+ centre is ligated by P_2 units only. If there was an interaction between two or more P_2 units, it would be weak relative to the Os^+–P_2 interaction. By analogy, we assume PH units to be present in the cations $OsPH^+$, OsP_3H^+ and so on.

PH_4^+ was generated in small amounts but could not be traced back to a particular metal-containing precursor by double-resonance experiments.

In addition to the species already addressed, ions not fitting into the reaction scheme outlined in sequence (4), namely OsH^+, OsP^+, OsP_2H^+, OsP_3^+, OsP_4H^+, OsP_5^+ and OsP_6H^+, were detected. With their total intensity not exceeding six per cent of the total ion intensity, these ions constitute a minor reaction channel. Remarkably, this minor reaction pathway may be described as being "shifted" with respect to the major reaction channel by just one hydrogen atom. On other words, inclusion of the reaction $Os^+ \xrightarrow[+PH_3,\ -PH_2]{k_{00\rightarrow01}} OsH^+$ into the kinetic model allows for keeping the maximum dehydrogenation paradigm. We think that the minor reaction channel may originate from either electronically excited osmium monocations or normal branching from electronic ground-state osmium monocations. While the ions of interest were subject to low signal-to-noise ratios, it was possible to obtain at least qualitative estimates for their formation and consumption rates. These rate constants and those of the major reaction channel are in the same order of magnitude (see Table 5); this makes us favour the "normal branching" explanation.

Iridium: The reaction sequence for iridium follows that given in scheme (4) from Ir^+ through to IrP_6^+. Similar to RuP_6^+ and OsP_6^+, the IrP_6^+ ion reaches a maximum of about 70% of the total ion intensity at a certain reaction time. However, in contrast to RuP_6^+ and OsP_6^+, the temporal evolution of IrP_6^+ could be adequately described by a simple generation–consumption scheme. Observed species not mentioned in sequence (4) were $IrP_2H_2^+$ and $IrP_4H_2^+$. However, as these two species did not occur in substantial concentrations nor did they accumulate, we assume them to loose molecular hydrogen easily; thus, "joining" the major reaction pathway. For obvious reasons, it is not possible to obtain meaningful rate constants for generation of the hydrogen-rich species $IrP_2H_2^+$ and $IrP_4H_2^+$ and their decomposition to yield the corresponding hydrogen-poor species IrP_2^+ and IrP_4^+, respectively. A branching ratio between the major reaction pathway $IrPH^+ \xrightarrow[+PH_3,\ -2H_2]{k_{11\rightarrow20}} IrP_2^+$ and its minor counterpart $IrPH^+ \xrightarrow[+PH_3,\ -H_2]{k_{11\rightarrow22}} IrP_2H_2^+ \xrightarrow[-2H_2]{k_{22\rightarrow20}} IrP_2^+$ favouring the latter one will increase both $k_{11\rightarrow22}$ and $k_{22\rightarrow20}$ as follows from applying Bodenstein's "stationary concentration" principle to the $IrP_2H_2^+$ ion. A related argument applies to the determination of the rate constants for the $IrP_3H^+ \xrightarrow[+PH_3,\ -H_2]{k_{31\rightarrow42}} IrP_4H_2^+ \xrightarrow[-2H_2]{k_{42\rightarrow40}} IrP_4^+$ subsystem of reactions. Consequently, the species $IrP_2H_2^+$ and $IrP_4H_2^+$ were disregarded in the kinetic analysis (see Table 3) altogether with the reactions either producing or consuming them. However, formation and consumption of the hydrogen-poor species IrP_2^+ and IrP_4^+, respectively, was included. As a consequence, the rate constants $k_{11\rightarrow20}$ and $k_{31\rightarrow40}$ reported here account for both the major and the minor reaction pathways mentioned.

Beyond IrP_6^+, the character of the system changes: 1) both hydrogen-poor (namely IrP_7H^+ and IrP_8^+) and hydrogen-rich species (namely $IrP_7H_3^+$, $IrP_8H_2^+$, $IrP_8H_6^+$, $IrP_9H_3^+$ and $IrP_9H_5^+$) were observed, 2) the temporal evolution of the IrP_7H^+ ion could not be modelled by a simple generation–consumption scheme except when allowing for a much faster consumption of the IrP_6^+ ion than experimentally observed. When undertaking double-resonance experiments for the observed species, we did not repeat the full-detailed double-resonance study undertaken for the Ru^+/PH_3 system, but instead adopt the above scheme by analogy. The reaction sequence is summarized in scheme (16). Species not observed in kinetic measurements are given in parentheses. Reaction channels not investigated are given in parentheses as well.

Table 5. Reaction rates and efficiencies for the Os^+/PH_3 system.[a,b]

Reaction channel[c,d]	Rate constant						
non-(4)	$k_{00\rightarrow01}$ 8.8×10^{-12} (0.79%)	$k_{01\rightarrow10}$ 4.0×10^{-10} (35%)	$k_{10\rightarrow21}$ 6.3×10^{-10} (57%)	$k_{21\rightarrow30}$ 9.4×10^{-10} (85%)	$k_{30\rightarrow41}$ 8.9×10^{-10} (82%)	$k_{41\rightarrow50}$ 7.4×10^{-10} (78%)	$k_{50\rightarrow61}$ 6.4×10^{-10} (59%)
(4)		$k_{00\rightarrow11}$ 5.0×10^{-10} (45%)	$k_{11\rightarrow20}$ 5.0×10^{-10} (45%)	$k_{20\rightarrow31}$ 6.0×10^{-10} (55%)	$k_{31\rightarrow40}$ 7.0×10^{-10} (65%)	$k_{40\rightarrow51}$ 7.8×10^{-10} (72%)	$k_{51\rightarrow60}$ 2.8×10^{-10} (26%)
(5)/(6)		$k_{60\rightarrow73}$ 4.7×10^{-11} (4.4%)	$k_{71\rightarrow82}$ 1.1×10^{-10} (11%)	$k_{73\rightarrow71}$ $0.26\ s^{-1}$	$k_{73\rightarrow86}$ n.d.[b]		
(5)/(6)		$k_{80\rightarrow91}$ n.d.	$k_{80\rightarrow93}$ n.d.	$k_{82\rightarrow80}$ $0.057\ s^{-1}$	$k_{82\rightarrow93}$ n.d.	$k_{82\rightarrow95}$ n.d.	

[a] Unless otherwise noted, *reaction rates* are given in units of $cm^3 molecules^{-1} s^{-1}$, whereas *reaction efficiences* ϕ (values given in parentheses) are given as fractions of the experimentally observed rate constant and that according to the capture theory,[19] $\phi = k_{exp}/k_{cap} \times 100\%$. [b] n.d. = not determined, see text. [c] The numbers correspond to the reaction sequences numbers given in the text. [d] For a distinction between the reaction channels "non-(4)" and "(4)", see text.

0947-6539/02/0809-2062 $ 20.00+.50/0 *Chem. Eur. J.* **2002**, *8*, No. 9

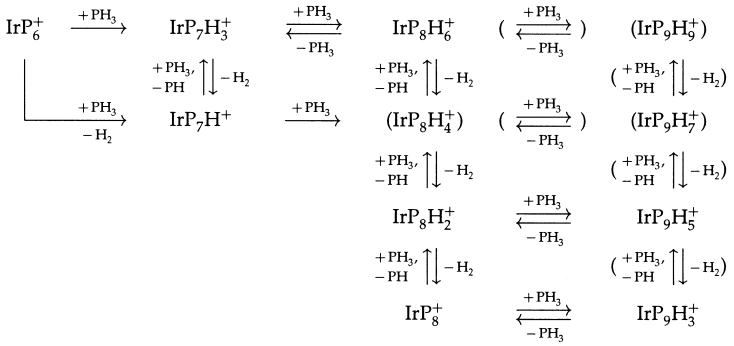

(16)

Due to 1) the fact that the temporal evolution of the IrP_7H^+ ion cannot be modelled by a simple generation–consumption scheme, 2) the manifold of possible reactions of the Ir^+/PH_3 system beyond IrP_6^+ [see sequence (16)] and 3) in anticipation of gain of little knowledge only the detailed kinetic modelling of the Ir^+/PH_3 system beyond the consumption of IrP_6^+ was not undertaken. The rate constant $k_{60\rightarrow71}$ reported here is actually the sum of $k_{60\rightarrow71}$ and much smaller $k_{60\rightarrow73}$. Upon its determination, the sole focus was on the temporal development of the IrP_6^+ ion, whereas the rise of the product ions IrP_7H^+ and $IrP_7H_3^+$ was not paid attention to. The essential findings for the Ir^+/PH_3 system beyond IrP_6^+ are that 1) dehydrogenation is no longer complete for $IrP_mH_n^+$ ions ($m \geq 7$), 2) nonetheless, maximum dehydrogenation occurs and dominates the product spectrum up to IrP_8^+, 3) beyond IrP_8^+, adduct formation is observed and 4) IrP_7H^+ initially dominates over $IrP_7H_3^+$ by a ratio of up to 20:1, but is consumed faster than $IrP_7H_3^+$. For species $IrP_8H_n^+$, IrP_8^+ dominates over $IrP_8H_2^+$ and the late-occuring $IrP_8H_6^+$. In fact, IrP_8^+ takes the lead from IrP_6^+, while the concentration maximum of the IrP_7H^+ ion falls short of those of all ions mentioned in the major reaction sequence [sequence (4)], except the non-observed IrP_9H^+. Finally, $IrP_9H_3^+$ dominates over $IrP_9H_5^+$.

Platinum: Driven by the observation of hydrogen-rich species $MP_mH_n^+$ ($n > m \bmod 2$) for second- and third-row transition metals, we reinvestigated the Pt^+/PH_3 system and observed a great manifold of products and a variety of reactions that interconvert them. In the following, these observations shall be presented in a systematic way.

1) The results reported by Brönstrup et al.[7] were confirmed in so far as the "maximum dehydrogenation" pathway [reaction scheme (17), major pathway] dominates the reaction sequence. In addition, the $PtPH^+$ ion gives rise to hydrogen-rich species (minor pathway). Furthermore, PH_4^+ was found to reach 3–4% of the total ion concentration and to be generated from, at least in part, to the species PtP_3H^+, $PtP_4H_3^+$, PtP_5H^+ and, probably, $PtPH^+$.

2) For ions containing at least four phosphorus atoms, a great manifold of hydrogen-rich species was observed. Double-resonance experiments revealed numerous interconversion reactions as shown in sequences (18)–(20). We would like to point out that this diversity of reactions observed for species $PtP_mH_n^+$ ($m \geq 4$) has no equivalent in the other M^+/PH_3 systems investigated in this study. However, the variety of both hydrogen-rich species and reactions interconverting them does not tell us anything about their particular significances. As a matter of fact, the ions constituting the major reaction pathway shown in scheme (17) account for at least 66% of the total ion intensity throughout the entire reaction. Table 6 demonstrates the ions' significance in more detail. As shown, ten ions account for at least 90% of the total ion intensity, whereas thirteen ionic species account for at least 95% of it. It should be noted that these thirteen ions account for the total ion intensity at reaction times of 64, 128, and 192 s. Thus, neglecting other ions (namely $PtP_2H_3^+$ and $PtP_3H_3^+$) on the basis of Table 6 would affect intermediates and not final products. We will refer to this point later.

3) The interpretation of the double-resonance experiments is not trivial. For example, ejection of PtP_6^+ from the reaction cell caused the signals of $PtP_6H_3^+$ and $PtP_6H_6^+$ to decrease significantly. Similarily, ejection of $PtP_6H_3^+$ caused the signal of $PtP_6H_6^+$ to decrease significantly. In a straightforward manner, one might interpret this experimental result as being caused by the reaction sequence

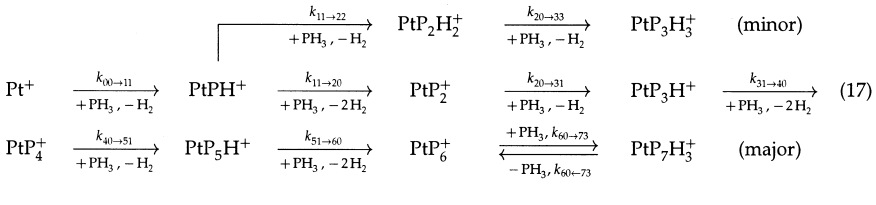

(17)

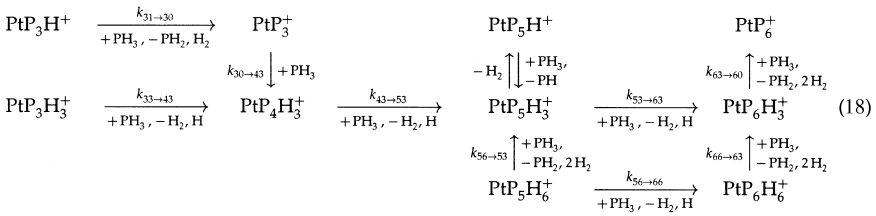

(18)

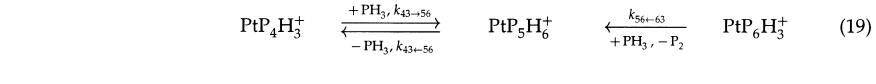

(19)

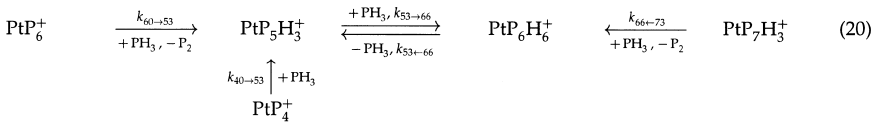

(20)

Table 6. Ion concentrations for the Pt^+/PH_3 system.[a–c]

Line	Ions	Reaction time [s]												
		0	1	2	3	4	6	8	16	24	32	64	128	192
1	Pt^+	100	80	63	50	42	26	18	2	0	0	0	0	0
2	scheme (4), major pathway	100	100	100	100	97	98	97	89	85	82	71	70	66
3	line 2+PH_4^+	100	100	100	100	100	100	98	93	89	86	75	73	69
4	line 3+$Pt_5H_3^+$	100	100	100	100	100	100	98	93	92	94	89	87	83
5	line 4+$Pt_6H_6^+$	100	100	100	100	100	100	98	93	92	94	90	91	89
6	line 5+$Pt_4H_3^+$	100	100	100	100	100	100	98	95	96	98	96	95	92
7	line 6+$Pt_5H_6^+$	100	100	100	100	100	100	98	95	96	98	97	97	97
8	line 7+$Pt_6H_3^+$	100	100	100	100	100	100	98	95	96	98	100	100	100
9	line 8+$Pt_2H_2^+$	100	100	100	100	100	100	100	96	96	98	100	100	100
10	line 9+$Pt_3H_3^+$	100	100	100	100	100	100	100	98	97	98	100	100	100
11	line 10+$Pt_4H_2^+$	100	100	100	100	100	100	100	100	100	100	100	100	100

[a] Phosphane pressure: 1.0×10^{-8} mbar, maximum reaction time: 192 s. [b] All data normalised to Σ(ion concentration) = 100. [c] For a reaction time of 0 s, only Pt^+ was observed.

$PtP_6^+ \xrightarrow[+PH_3,\,-P]{k_{60\rightarrow63}} PtP_6H_3^+ \xrightarrow[+PH_3,\,-P]{k_{63\rightarrow66}} PtP_6H_6^+$. However, this sequence would require loss of atomic phosphorus which is unlikely to occur according to thermochemical data (Table 1). Furthermore, such processes would contradict all previous experiments undertaken in this study which showed, if at all, only loss of molecular (P_2) phosphorus from the metal centres. Consequently, we explain the above-mentioned experimental findings by other reaction pathways as shown in expressions (21) – (23). One might argue that the loss of atomic hydrogen in the reaction $PtP_5H_3^+ \xrightarrow[+PH_3,\,-H_2,H]{k_{55\rightarrow63}} PtP_6H_3^+$ is as unlikely as the loss of atomic phosphorus. However, we think that the formation of a P_2 unit ligating the platinum centre combined with "boiling off" H_2 and H from PH units and/or

$$PtP_6^+ \xrightarrow[+PH_3\,,\,-P_2]{k_{60\rightarrow53}} PtP_5H_3^+ \xrightarrow[+PH_3\,,\,-H_2,H]{k_{53\rightarrow63}} PtP_6H_3^+ \quad (21)$$

$$PtP_6H_3^+ \xrightarrow[+PH_3\,,\,-P_2]{k_{63\rightarrow56}} PtP_5H_6^+ \xrightarrow[+PH_3\,,\,-H_2,H]{k_{56\rightarrow66}} PtP_6H_6^+ \quad (22)$$

$$PtP_6^+ \xrightarrow[+PH_3]{k_{60\rightarrow73}} PtP_7H_3^+ \xrightarrow[+PH_3\,,\,-P_2]{k_{73\rightarrow66}} PtP_6H_6^+ \quad (23)$$

PH_3 is favoured on both energetic (Table 1) and entropic grounds. In addition, the proposed reactions, for example, $PtP_7H_3^+ \xrightarrow[+PH_3,\,-P_2]{k_{73\rightarrow66}} PtP_6H_6^+$, allow for maintaining a PtP_4^+ core with either two P_2 units or one P_4 unit being bound to the metal centre.

4) The P_2/PH_3 ligand exchange is remarkable. With the exception of the other d^9 cation Pd^+, this type of reaction has not been observed in our study.

5) The frequent switching between "open-shell" species $PtP_mH_n^+$ (odd $(m + n)$) and their "closed-shell" counterparts (even $(m + n)$) is unique among the M^+/PH_3 systems investigated in this study.

For a kinetic analysis, the reaction schemes (17) – (20) pose the problem of maldetermination of certain rate constants. For example, $PtP_4H_3^+$ is formed in three reactions and consumed in two, which are, in turn, interconnected by other reactions. Consequently, an apparently good fit of the observed species' temporal evolution can be obtained irrespective of the rate constants' true significance.

For a simplification of reaction schemes (17) – (20), we proceeded as follows. 1) The most important reaction channel [scheme (17), major pathway] was kept. 2) The reaction channel $PtP_3H^+ \xrightarrow[+PH_3,\,-PH_2,H_2]{k_{31\rightarrow30}} PtP_3^+ \xrightarrow[+PH_3]{k_{30\rightarrow43}} PtP_4H_3^+$ was neglected, because PtP_3^+ was not observed in the kinetic studies and, furthermore, the transformation $PtP_3H^+ \xrightarrow[+PH_3,\,-PH_2,H_2]{k_{31\rightarrow30}} PtP_3^+$ would be the only one of this type in the entire reaction scheme. As a consequence, the "hydrogen-rich" reaction channel [scheme (17), minor pathway] had to be kept to account for the formation of $PtP_4H_3^+$. The formal P-atom addition reaction $PtP_3H_3^+ \xrightarrow[+PH_3,\,-H_2,H]{k_{33\rightarrow43}} PtP_4H_3^+$ occurring in this reaction channel is paralleled by similar reactions of $PtP_5H_3^+$ and $PtP_5H_6^+$. 3) The hydrogen addition reaction $PtP_5H^+ \xrightarrow[+PH_3,\,-PH]{k_{51\rightarrow53}} PtP_5H_3^+$ was neglected based on its rather small influence established by the double-resonance experiments. For the same reason, the reactions $PtP_5H_6^+ \xrightarrow[+PH_3,\,-PH_2,2H_2]{k_{56\rightarrow53}} PtP_5H_3^+$, $PtP_6H_6^+ \xrightarrow[-PH_3]{k_{53\rightarrow66}} PtP_5H_3^+$ and $PtP_6H_6^+ \xrightarrow[+PH_3,\,-PH_2,2H_2]{k_{66\rightarrow63}} PtP_6H_3^+$ were neglected. The rate constants for these reactions are marked as "not determined" in Table 7. 4) All other reactions were included in the kinetic model. This model involves fifteen species, eighteen simple and two equilibrium reactions and is shown below in expressions (24) – (28). In order to ease comparison with the nonsimplified reaction scheme [expressions (17) – (20)], we keep the arrangement of the species' formulae. While still containing a wide variety of conversion reactions, the simplified model constitutes a compromise between simplicity and full coverage of the investigated system.

By applying this reaction scheme, the temporal evolution of almost all species considered can be reproduced well by

$$\begin{array}{ccccccccccc} & & & & & \xrightarrow[+PH_3\,,\,-H_2]{k_{11\rightarrow22}} & PtP_2H_2^+ & \xrightarrow[+PH_3\,,\,-H_2]{k_{20\rightarrow33}} & PtP_3H_3^+ & & \\ Pt^+ & \xrightarrow[+PH_3\,,\,-H_2]{k_{00\rightarrow11}} & PtPH^+ & \xrightarrow[+PH_3\,,\,-2H_2]{k_{11\rightarrow20}} & PtP_2^+ & \xrightarrow[+PH_3\,,\,-H_2]{k_{20\rightarrow31}} & PtP_3H^+ & \xrightarrow[+PH_3\,,\,-2H_2]{k_{31\rightarrow40}} & & & \\ PtP_4^+ & \xrightarrow[+PH_3\,,\,-H_2]{k_{40\rightarrow51}} & PtP_5H^+ & \xrightarrow[+PH_3\,,\,-2H_2]{k_{51\rightarrow60}} & PtP_6^+ & \underset{-PH_3,\,k_{60\leftarrow73}}{\overset{+PH_3,\,k_{60\rightarrow73}}{\rightleftharpoons}} & PtP_7H_3^+ & & & & \end{array} \quad (24)$$

0947-6539/02/0809-2064 $ 20.00+.50/0 *Chem. Eur. J.* **2002**, *8*, No. 9

Table 7. Reaction rates and efficiencies for the Pt^+/PH_3 system.[a,b]

(Formal) reaction	Rate constant					
(4)	$k_{00\rightarrow11}$	$k_{11\rightarrow20}$	$k_{20\rightarrow31}$	$k_{31\rightarrow40}$	$k_{40\rightarrow51}$	$k_{51\rightarrow60}$
ref. [7]	6.0×10^{-10}	7.5×10^{-10}	3.3×10^{-10}	5.5×10^{-10}	1.2×10^{-10}	4.0×10^{-10}
	6.6×10^{-10}	7.8×10^{-10}	4.1×10^{-10}	6.9×10^{-10}	1.3×10^{-10}	4.3×10^{-10}
	(59%)	(71%)	(37%)	(63%)	(12%)	(40%)
	$k_{60\rightarrow73}$	$k_{60\leftarrow73}$				
	6.7×10^{-12}	n.r.[d,e]				
	(0.63%)					
PH_3 addn./loss	$k_{30\rightarrow43}$	$k_{40\rightarrow53}$	$k_{43\rightarrow56}$	$k_{43\leftarrow56}$	$k_{53\rightarrow66}$	$k_{53\leftarrow66}$
	n.d.[c]	2.4×10^{-11}	n.r.	$8.9\times10^{-4}\ s^{-1}$	8.8×10^{-12}	n.d.
		(2.3%)			(0.82%)	
H_n addn./loss	$k_{31\rightarrow30}$	$k_{51\rightarrow53}$	$k_{53\rightarrow51}$	$k_{56\rightarrow53}$	$k_{63\rightarrow60}$	$k_{66\rightarrow63}$
	n.d.	n.d.	$3.4\times10^{-3}\ s^{-1}$	n.d.	n.r.	n.d.
P_2/PH_3 exch.	$k_{60\rightarrow53}$	$k_{56\leftarrow63}$	$k_{66\leftarrow73}$			
	8.5×10^{-12}	4.9×10^{-11}	n.d.			
	(0.79%)	(4.5%)				
P addn.	$k_{33\rightarrow43}$	$k_{43\rightarrow53}$	$k_{53\rightarrow63}$	$k_{56\rightarrow66}$		
	6.9×10^{-10}	n.r.	1.6×10^{-11}	5.1×10^{-12}		
	(64%)		(1.5%)	(0.47%)		

[a] Unless otherwise noted, all data are taken from this work. [b] Unless otherwise noted, *reaction rates* are given in units of $cm^3\,molecules^{-1}\,s^{-1}$, whereas *reaction efficiences* ϕ (values given in parentheses) are given as fractions of the experimentally observed rate constant and that according to the capture theory,[19] $\phi = k_{exp}/k_{cap}\times100\%$. [c] n.d. = not determined, see text. [d] n.r. = no reactivity indicating a reaction efficiency $\phi < 0.01\%$. [e] The modelling program[18] returned a rate constant of zero.

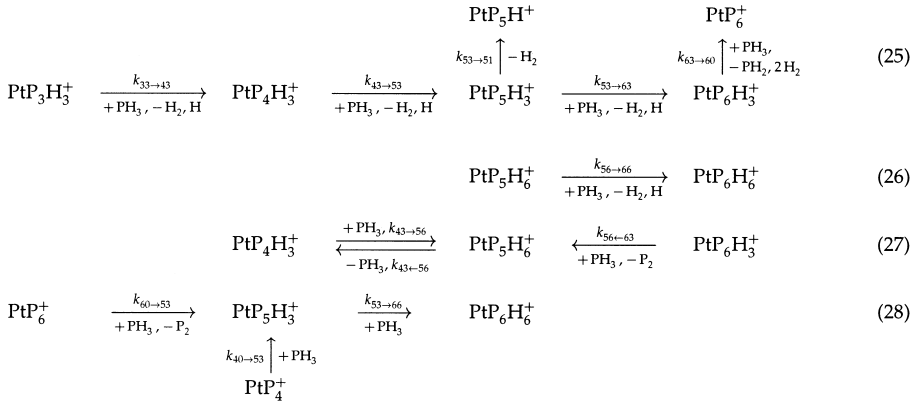

22 elementary reactions and their respective rate constants. While the only significant deviation between the experimental and the modelled data occurs for $PtP_7H_3^+$, whose formation is too fast initially, we would like to point out that the agreement with the rate constants reported in ref. [7] is good to excellent. This proves, in our opinion, the dominance of the major reaction pathway, whose reaction rate constants can be said to be exact within the experimental error. On the other hand, the rate constants for the reations (25) – (28) should be taken as reasonable estimates rather than exact values due to the uncertainty introduced by the complex reaction scheme.

Conclusion

In this study, we have investigated the reactions of the Group 8, 9, and 10 transition metal monocations with phosphane. First-row transition metal monocations are not very reactive towards PH_3 with background-mediated adduct formation being the predominant chemical reaction. In contrast, second- and third-row transition metal monocations are fairly reactive towards phosphane. With the exception of palladium whose reaction termini are $PdPH_3^+$, $PdP_2H_6^+$ and $PdP_2H_3^+$, all other ions (Ru^+, Rh^+, Os^+, Ir^+ and Pt^+) follow the "maximum dehydrogenation" pathway yielding MPH^+, MP_2^+, MP_3H^+, MP_4^+, MP_5H^+ and MP_6^+ as major product ions. According to collision-induced dissociation experiments, P_2 and PH units are preferably formed as ligands. At the stage of MP_6^+ (M = Ru, Rh, Ir, Pt) or MP_7H^+ (M = Os), the character of the system changes: 1) the temporal evolution of the cation just mentioned cannot be modelled by simple generation – consumption schemes, 2) further reactions with PH_3 do not necessarily form maximally dehydrogenated species and 3) numerous hydrogen-exchange equilibrium reactions between the product ions and PH_3 are observed. For the d^9 cations of Pd^+ and Pt^+, a remarkable weakness of the M^+–P_2 bond is noted.

Experimental Section

Phosphane (Praxair, "electronic grade" 99.995%) and argon (Praxair, 99.996%) were obtained commercially and used without further purification.

All experiments were performed with a Bruker Spectrospin CMS-47X Fourier-transform ion cyclotron resonance (FT-ICR) mass spectrometer, whose setup and operation have been described previously.[11, 12] In brief, atomic monocations M^+ (M = Fe, Co, Ni, Ru, Rh, Pd, Os, Ir, Pt) were generated from targets of the respective pure metal by laser desorption/laser ionization[13,14] in the external ion source of the spectrometer by using a Nd:YAG laser (Spectron Systems; $\lambda_{max} = 1064$ nm). The metal ions were extracted from the source and transferred to the analyser cell by a system of electrostatic potentials. Next, the most abundant isotope (^{56}Fe, ^{58}Ni, ^{102}Ru, ^{106}Pd, ^{192}Os, ^{193}Ir, ^{195}Pt; ^{59}Co and ^{103}Rh are isotopically pure elements) was

mass-selected using FERETS,[15] a computer-controlled ion-ejection protocol that combines frequency sweeps and single-frequency pulses to optimise resonant excitation and ejection of all unwanted ions. After mass selection, the metal ions were allowed to thermalise by multiple collisions with pulsed-in argon. Whereas the normal background pressure was about $(2-3)\times10^{-9}$ mbar (1 mbar $=10^2$ Pa) in the analyser cell of our spectrometer, the argon pressure was allowed to reach $10^{-5}-10^{-4}$ mbar. According to the purely exponential decay of their concentrations in the kinetic studies, the metal cations were assumed to be completely thermalised. Phosphane was admitted to the cell through a leak valve at a constant pressure measured by a calibrated BALZERS IMG 070 ion gauge.[16] Unless otherwise mentioned, the phosphane pressure was $(1-9)\times10^{-8}$ mbar.

The elemental compositions of ions were established by high-resolution mass spectrometry in combination with the signal-matching capability of the spectrometer-controlling ASPECT 3000 microcomputer.

Reaction mechanisms were derived from kinetic arguments and complementary double-resonance experiments.[17] In a double-resonance experiment, a particular ion is ejected from the analyser cell by resonant excitation for a certain amount of time. The resulting spectrum is compared to a reference spectrum obtained by "ejecting" a hypothetical ion (for example, $m/z=200$) for the same amount of time. Disappearance of an ion indicates that it is formed, directly or indirectly, from the ejected ion. Rate constants were determined by using a computer program that determines rate constants of consecutive and parallel reactions based on a flexible kinetic model and experimentally observed ion intensities.[18] The reported rate constants are given as fractions of the measured bimolecular rate constants and the gas kinetic collision rates according to the capture theory.[19] The parameters used for phosphane were: dipole moment 0.574 D,[20] polarisability 4.84×10^{-24} cm^3,[20] relative ion gauge sensitivity 1.8 (estimated according to ref. [21]). The absolute error of the rate constants is in the range of $\pm30\%$, while the ratios of the rate constants are more precise ($\pm10\%$).[16] The metal monocation/phosphane reaction sequences were assumed to be complete when no changes of the product ion ratios were observed at long reaction times.

To elucidate the connectivity of ionic species, collision-induced dissociation (CID) experiments[22] were undertaken. In a CID experiment, the ion of interest is subjected to a pressure of typically $(1-4)\times10^{-8}$ mbar of a nonreacting gas (typically argon) after having been kinetically activated by a low-energy radio-frequency pulse. Eventual fragmentation reveals information about the ion's connectivity; to a certain extent, the respective bond strengths can be assessed from monitoring the fragments as a function of the energy of the radio-frequency excitation pulse.

By chance, a double-resonance experiment may come close to a CID experiment (see above). If, for example, a ligated metal ion is accelerated in order to be ejected from the cell, it may collide with reactant gas molecules at levels of energy exceeding RT and undergo collision-induced ligand loss. As a consequence, the corresponding fragments and/or their follow-up reaction products may gain intensity in double-resonance experiments.

Acknowledgement

This work was supported by the Deutsche Forschungsgemeinschaft, the Fonds der Chemischen Industrie and the Volkswagen-Stiftung. The authors also wish to thank the Degussa AG, Frankfurt/Main (Germany), for a generous gift of noble-metal targets and Dr. Detlef Schröder for fruitful discussion.

[1] N. L. Arthur, I. A. Cooper, *J. Chem. Soc. Faraday Trans.* **1997**, *93*, 521.
[2] J. Hrušak, D. Schröder, H. Schwarz, S. Iwata, *Bull. Chem. Soc. Jpn.* **1997**, *70*, 777.
[3] P. Antoniotti, L. Operti, R. Rabezzana, M. Splendore, G. Tonachini, G. A. Vaglio, *J. Chem. Phys.* **1997**, *107*, 1491.
[4] P. Antoniotti, L. Operti, R. Rabezzana, G. Tonachini, G. A. Vaglio, *J. Chem. Phys.* **1998**, *109*, 10853.
[5] U. Mazurek, H. Schwarz, *Inorg. Chem.* **2000**, *39*, 5586.
[6] M. Brönstrup, D. Schröder, H. Schwarz, *Chem. Eur. J.* **1999**, *5*, 1176.
[7] M. Brönstrup, D. Schröder, H. Schwarz, *Organometallics* **1999**, *18*, 1939.
[8] P. F. Greenwood, I. G. Dance, K. J. Fisher, G. D. Willett, *Inorg. Chem.* **1998**, *37*, 6288.
[9] Z. Gang, K. Su, Y. Wang, Z. Wen, *Chem. Phys.* **1998**, *228*, 31.
[10] S. G. Lias, J. E. Bartmess, J. F. Liebman, J. L. Holmes, R. D. Levin, W. G. Mallard, *J. Phys. Chem. Ref. Data Suppl. 1* **1988**, *17*, 1.
[11] K. Eller, H. Schwarz, *Int. J. Mass Spectrom. Ion Processes* **1989**, *93*, 243.
[12] K. Eller, W. Zummack, H. Schwarz, *J. Am. Chem. Soc.* **1990**, *112*, 621.
[13] B. S. Freiser, *Talanta* **1985**, *32*, 697.
[14] B. S. Freiser, *Anal. Chim. Acta* **1985**, *178*, 137.
[15] R. A. Forbes, F. H. Laukien, J. Wronka, *Int. J. Mass Spectrom. Ion Processes* **1988**, *83*, 23.
[16] D. Schröder, H. Schwarz, D. E. Clemmer, Y. Chen, P. B. Armentrout, V. I. Baranov, D. K. Böhme, *Int. J. Mass Spectrom. Ion Processes* **1997**, *161*, 175.
[17] M. B. Comisarow, V. Grassi, G. Parisod, *Chem. Phys. Lett.* **1978**, *57*, 413.
[18] U. Mazurek, H. Schwarz, ICR Kinetics, version 3.0.1, TU Berlin, Berlin, **1998**.
[19] T. Su, W. J. Chesnavich, *J. Chem. Phys.* **1982**, *76*, 5183.
[20] *CRC Handbook of Chemistry and Physics*, 79th ed. (Ed.: D. R. Lide), CRC, Boca Raton, FL, **1998**.
[21] J. E. Bartmess, R. M. Georgiadis, *Vacuum* **1983**, *33*, 149.
[22] I. Kretzschmar, D. Schröder, H. Schwarz, C. Rue, P. B. Armentrout, *J. Phys. Chem. A* **1998**, *102*, 10060.

Received: November 5, 2001 [F3654]

  0947-6539/02/0809-2066 $ 20.00+.50/0